International Journal of Extreme Automation and Connectivity in Healthcare
Volume 1 • Issue 2 • July-December 2019

On the Separation of Normal and Abnormal Stem Cell-Derived Cardiomyocytes' Calcium Transient Signals

Martti Juhola, Tampere University, Tampere, Finland
Henry Joutsijoki, Tampere University, Tampere, Finland
Kirsi Varpa, Tampere University, Tampere, Finland
Kirsi Penttinen, Tampere University, Tampere, Finland
Katriina Aalto-Setälä, Tampere University, Tampere, Finland

ABSTRACT

A data set of 438 calcium transient signals measured from induced pluripotent stem cell derived cardiomyocytes was collected to analyze and separate abnormal signals corresponding to aberrant cardiomyocytes from normal signals corresponding to normally developed cells. After the calcium transient peak detection, the authors computed peak variable values. Each signal peak was determined to be either normal or abnormal. The peak variables were used for machine learning algorithms to classify entire calcium transient signals into normal or abnormal types. The authors evaluated the classification power of 10 variables to separate normal signals from abnormal ones. This article obtained classification accuracies of up to 85-95%, around 5% better than the results in the preliminary research. The correctness of the classification of the signals was inferred either by a biotechnology expert or by an algorithm. The new results are promising for the continuity of this area of study in identifying aberrant calcium transients.

KEYWORDS

Calcium Transient Signal, Cardiomyocyte, Classification, Genetic Cardiac Diseases, Induced Pluripotent Stem Cell, Machine Learning, Peak Recognition, Signal Analysis

INTRODUCTION

Calcium cycling refers to the release and reuptake of intracellular calcium, and it is the central regulator of cardiac contraction and relaxation. Cardiac contractility is determined by the amplitude and kinetics of calcium cycling and therefore it has a great impact on the functionality of cardiomyocytes. It is initiated by action potential, and leads to the excitation-contraction coupling of the cardiomyocytes (Marks, 2013). Aberrant calcium cycling due to cardiac diseases or different drugs can lead to abnormal calcium transients, which can cause impaired contractility and fatal cardiac arrhythmias. It is therefore important to understand and analyze cellular calcium cycling.

Calcium imaging of cardiomyocytes is a method for monitoring calcium cycling activity *in vitro*. In recent years, the calcium cycling functionality of cardiomyocytes has been studied widely with induced pluripotent stem cell (iPSC) (Marks, 2013) -derived cardiomyocytes. Typically, the cells

DOI: 10.4018/IJEACH.2019070102

are generated from patients carrying different genetic cardiac disorders, and they offer a promising platform for studying the pathophysiology of various disorders and drug responses in human cells. These previous studies have offered new insights into different cardiac diseases by revealing substantial defects and abnormalities in the calcium cycling of these cardiomyocytes, reflecting the cardiac phenotype observed in patients (Takahashi et al., 2007; Penttinen et al., 2015a; Fatima et al., 2011; Jung et al., 2012; Kujala et al., 2012; Lan et al., 2013; Kiviaho et al., 2015; Ojala et al., 2016; Penttinen et al., 2015b). Recently studied diseases revealing calcium cycling abnormalities include catecholaminergic polymorphic ventricular tachycardia (CPVT), an exercise-induced malignant arrhythmogenic disorder (Penttinen et al., 2015a; Kujala et al., 2012), long QT syndrome 1 (LQT1), an electric disorder of the heart that predisposes patients to arrhythmias and sudden cardiac death (Kiviaho et al., 2015), and hypertrophic cardiac myopathy (HCM), a disorder that affects the structure of heart muscle tissue leading to arrhythmias and progressive heart failure (Ojala et al., 2016).

To accelerate the development, application, research, and innovations of stem cell-derived cardiomyocytes, we study the automatic separation of CPVT-, LQT1-, HCM-specific and control (WT) iPSC-derived cardiomyocytes into normal and abnormal groupings to distinguish aberrant cells from normally developed cells. This can be implemented by separating individual cells according to their calcium cycling. Thus far, this separation has been performed manually by biotechnologists or medical laboratory personnel. To gradually enable progress from theoretical research to medical practice, appropriate software based on signal analysis, pattern recognition, and machine learning algorithms is needed to automatize some of the routine-like but very demanding work of biotechnological experts.

BACKGROUND

The study was approved by the Ethics Committee of Pirkanmaa Hospital District (R08070). Patient-specific iPSC lines were established and characterized as described earlier (Penttinen et al., 2015a; Kiviaho et al., 2015; Ojala et al., 2016; Juhola et al., 2015). The studied iPSC lines were UTA.05605.CPVT, UTA.05208.CPVT, UTA.07001.CPVT, UTA.03701.CPVT, UTA.05503.CPVT, and UTA.05404.CPVT generated from CPVT patients carrying cardiac ryanodine receptor (RyR2) mutations; UTA.07801.HCMM, and UTA.06108.HCMM generated from HCM patients carrying α-tropomyosin (TPM1) and myosin-binding protein C (MYBPC3)) mutations; UTA.00208.LQT1 and UTA.00118.LQT1 generated from LQT1 patients carrying potassium voltage-gated channel subfamily Q member 1 (KCNQ1) mutations; and UTA.04602.WT generated from healthy control individuals (Table 1). IPSCs were differentiated into spontaneously beating cardiomyocytes and dissociated into coverslips for calcium imaging studies, which was conducted in spontaneously beating Fura-2 AM-loaded (Invitrogen, Molecular Probes) cardiomyocytes as described earlier (Penttinen et al., 2015a; Juhola et al., 2015). For calcium analysis, regions of interest were selected for spontaneously beating cells, and background noise was subtracted before further processing. Signals were acquired as the ratio of the emissions at 340/380 nm wavelengths.

The recognition of a peak in a calcium transient signal consists of finding its beginning, maximum, and end. Very small spikes with low amplitude and short duration are seen as noise and ignored. If the amplitude of a small spike is smaller than approximately 8% of the average amplitude estimate of large peaks of the signal analyzed, such a spike is defined to be noise, in other words, no actual peak. The recognition of peaks is based on first computing the approximated first derivative signal and second using appropriate thresholds for the derivative signal in order to recognize the beginning, maximum, and end of each peak. The suitable threshold values were found experimentally (Penttinen et al., 2015b; Juhola et al., 2015; Juhola et al., 2014).

Table 1. Cell lines used

Cell line	Diseases	Mutation
UTA.05605.CPVT	CPVT	RyR2* – exon 3 deletion
UTA.05208.CPVT	CPVT	RyR2 – P2328S
UTA.07001.CPVT	CPVT	RyR2 – T2538R
UTA.03701.CPVT	CPVT	RyR2 – L4115F
UTA.05503.CPVT	CPVT	RyR2 – Q4201R
UTA.05404.CPVT	CPVT	RyR2 – V4653F
UTA.00208.LQT1	LQT1	*KCNQ1** – G589D
UTA.00118.LQT1	LQT1	*KCNQ1* – ivs7-2A>G
UTA.07801.HCMM	HCM	MYBPC3*-Gln1061X
UTA.06108.HCMM	HCM	MYBPC3-Gln1061X
UTA.04602.WT	-	-

*Cardiac ryanodine receptor (RyR2), potassium voltage-gated channel subfamily Q member 1 (KCNQ1), myosin-binding protein C (MYBPC3), α-tropomyosin (TPM1)

First, the beginning of a peak is found when the first derivative values remain greater than the threshold. Second, the maximum (top) is detected when the first derivative values are close to zero. Third, the end of the peak is detected when the absolute first derivative values drop to less than another threshold.

Peaks are recognized for further analysis in order to determine whether they are normal or somehow distorted, in which case they are called abnormal. This is based on computing peak variables related to durations, amplitudes, and shapes of peaks. These variable values are compared with experimentally determined threshold values or bounds to draw conclusions as to whether a peak is normal or abnormal. Abnormal peaks differ from normal ones. Classification of an entire calcium transient signal is executed on the basis of all its individual peaks: if even a single peak is found to be abnormal, the whole signal is classified as abnormal.

MAIN FOCUS OF THE ARTICLE

Peak Recognition in Calcium Transient Signals

At the beginning, after removing (temporarily during the peak detection) a linear trend typically existing in a calcium transient signal two subsets of all samples of the signal are taken, i.e., the greatest values, approximately 15% of all the distribution and then the smallest values as another subset of around 15% of all values. The means of both subsets are computed separately. The difference of these average maximum and average minimum is used as the amplitude estimate of large amplitude peaks in the signal as follows. The abnormality of a peak is true if one of the following conditions is satisfied. See Figure 1-4 as examples. First, if the higher side amplitude of a peak in the signal is less than 65% from the higher side amplitude of the preceding large peak defined to be normal or at least large (greater than 50% of the large peak amplitude estimate), the current peak is decided to be abnormal (Figure 4, the red marks). However, if there is neither preceding normal peak nor any previous large peak or the current peak is the first one in the signal, the current peak is compared with 65% of the above-mentioned amplitude estimate of the large peaks. If the current peak is lower, then it is marked to be abnormal. Second, if the amplitude of one peak side is lower than 86% compared to the amplitude of its other side, this asymmetric peak is defined to be abnormal (Figure 2-4, the magenta marks). If neither the first nor

the second test did define a peak to be abnormal, the third one could still do it as follows. If the end location of a peak remained higher than 37% of the large peak amplitude estimate computed from the signal minimum amplitude (scaled to zero), such a peak would be defined to be abnormal. All percent values given here were formed experimentally using the data at our disposal.

In our preceding article on calcium transient signals (Juhola et al., 2015), we described the developed peak recognition procedure in detail as well as the classification of individual peaks into either normal or abnormal classes. Because we applied mostly the same peak recognition procedure here (some threshold values were only fine-tuned along with the extended data), we refer to our thorough description in (Juhola et al., 2015). In the current text, we concentrate on the classification of entire calcium transient signals in order to develop this classification further in terms of the efficiency of classification accuracy, in other words, to improve the separation of normal and abnormal calcium transient signals. We also studied whether the properties of transient signals of three different diseases differ from each other in normal and abnormal signals.

Data and Peak Variables

The signal data were measured with two programs. The older sampled data were measured at frequencies of approximately 8, 10, or 11 Hz and the newer data were measured at a frequency of 23 Hz. Altogether, 438 signals were measured, 133 with the older program and 305 with the newer one. The durations of signals varied from 7.7 s to 24 s with a mean of 16.0 s. These were short because the calcium imaging technique may damage the cells, thus the risk of phototoxicity limited their exposure time.

The numbers of peaks found by the peak recognition procedure varied from 1 to 45 peaks per signal. The average number was 13 peaks. In total, the signals contained 5,681 peaks. All peak recognition and signal classification programming was implemented with Matlab.

Figure 1. A normal calcium transient signal: all entire peaks recognized (the beginnings and ends found are marked with a blue mark) from a transient signal and assessed to be normal and labeled with a green mark at the top. (The first valid peak will be used in Figure 5.)

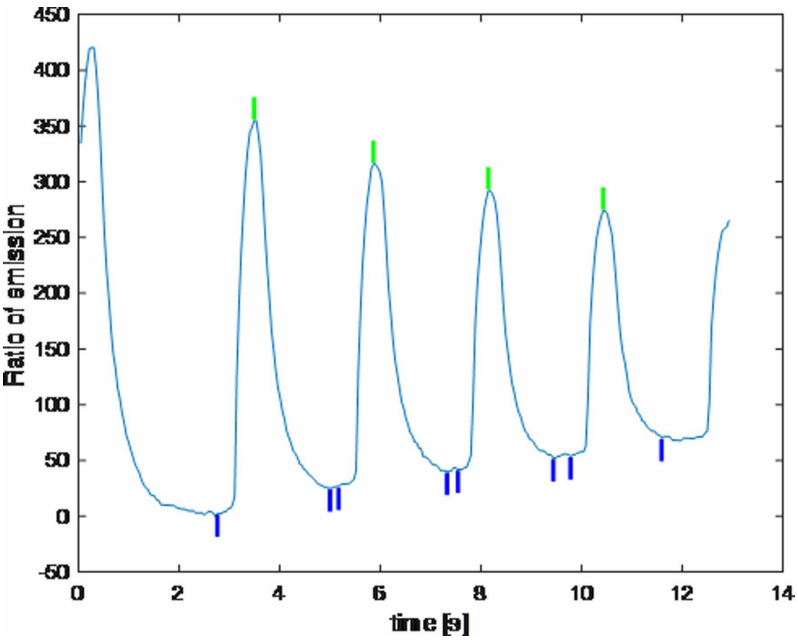

Figure 2.

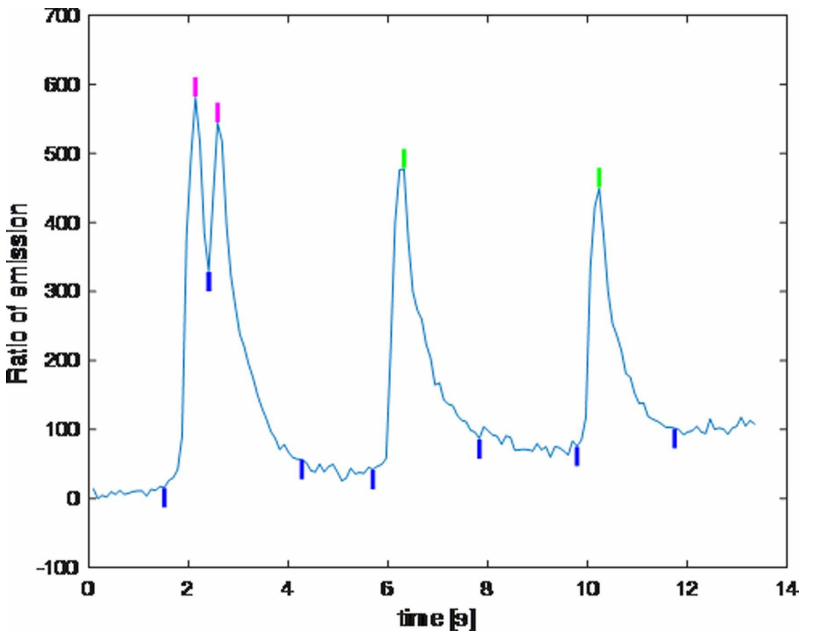

After the peak recognition, the variable values of every peak found from the signal were computed. The shapes and sizes of the peaks can vary greatly. A few examples are shown in Figure 1-4. The exact rules to define a peak to be normal or abnormal were given in our preceding article (Juhola et al., 2015). It is based on the use of the approximated first derivative of a signal: as simplified, peak minima and maxima recognized when the first derivative is close to zero or its sign changes from negative to positive or vice versa. The peaks found to be normal in Figure 1 and 3 are fairly "harmonious" and include no great shape or size differences between successive peaks. In other words, the heights of the left and right sides of the successive peaks are roughly same in every single peak, while the left side duration is frequently shorter than that of the right side. For the abnormal peaks, various irregularities can appear relating to the forms, sizes and also intervals between peaks computed from their maxima (tops). Note that the descending trend present in some calcium transient signals was removed from the signals in Figure 1-4 before recognizing their peaks. Nevertheless, the peak variable values were computed according to the original signals after the localization of peak beginnings, maxima, and ends. The trend removal was performed temporarily only to aid the peak recognition.

An abnormal calcium transient signal: the first occurrence as a "double peak" or two Figure 2. asymmetric peaks are distorted making the whole signal abnormal. The beginnings and ends found are marked with a blue mark. The peaks assessed to be normal are labeled with a green mark at the top and those to be abnormal (as asymmetric) labeled with a magenta mark.

After the recognition of the calcium transient peaks, their variables were computed. Figure 5(a) shows an example on the basis of which the peak variables used are described. Let us present signal $s(t)$ as the function of time and certain locations from a to g where a is the beginning and g the end of the peak. Seven variables were earlier applied (Juhola et al., 2015): the amplitudes (height) of peak left and right sides,

$$A_l = s(d) - s(a) \text{ and } A_r = s(d) - s(g),$$

Figure 3. An abnormal calcium transient signal: the first occurrence of an asymmetric peak is distorted with the peak sides of different heights, making the signal abnormal. All later peaks were assessed as normal.

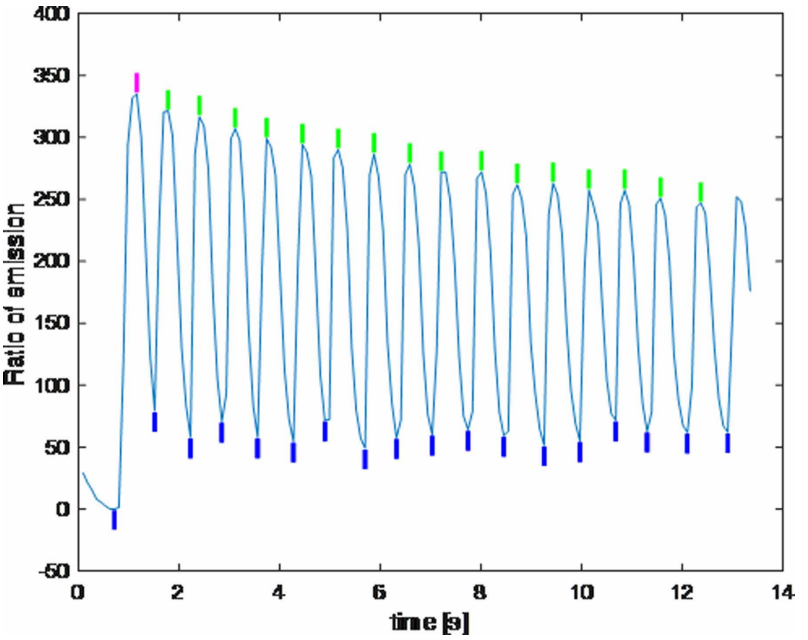

Figure 4. An abnormal calcium transient signal: all peaks but the last complete one found were determined to be abnormal because they were either "triple" or "double" peaks formed by asymmetric peaks labeled with a magenta mark at the top or too low amplitude peaks (compared to the other). Thus, the signal was abnormal.

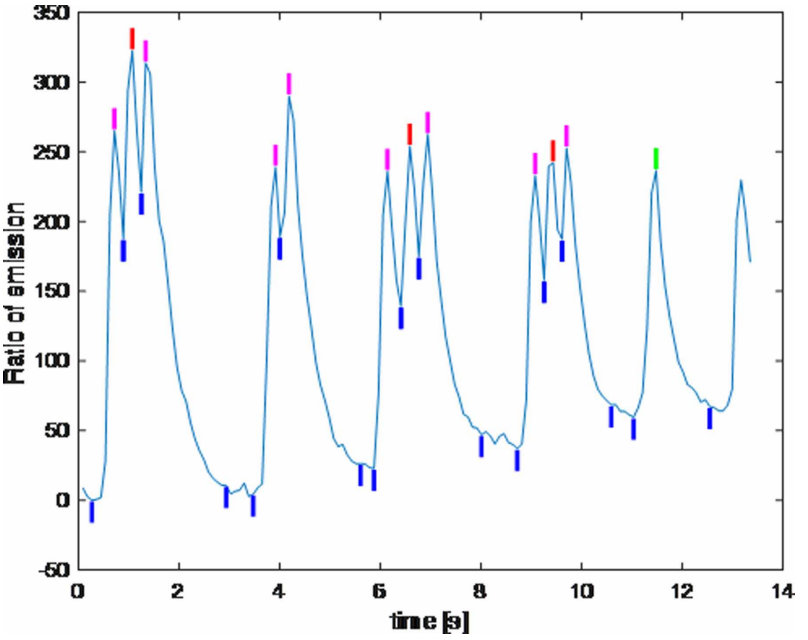

the durations of peak left and right sides (F sampling frequency)

$$D_l = \frac{d-a}{F} \quad \text{and} \quad D_r = \frac{g-d}{F},$$

the maximum of the 1st derivative of peak left side $s'(c)$, the absolute minimum of the 1st derivative of peak right side $s'(e)$, and the time difference from the current peak to the preceding one D_p. For the first peak of a signal, this is calculated from the signal beginning to the top of the peak.

In addition, three new variables are added: the maximum of the 2nd derivative of the peak right side $s''(f)$, the absolute minimum of the 2nd derivative of the peak right side $s''(d)$, and surface area R of the peak

$$R = \int_a^g s(t)\,dt - \left|\frac{(g-a)(s(g)-s(a))}{2F}\right|$$
$$\approx \sum_{i=1}^{n_j} \frac{s(i)+s(i-1)}{2F} - \left|\frac{(g-a)(s(g)-s(a))}{2F}\right|$$

Figure 5. (a) The second peak from the signal *s* in Figure 1 classified as normal. (b) Its approximated first derivative *s'* and (c) second derivative *s''*. The location of the beginning along with the time axis is *a* and the location of the end *g*.

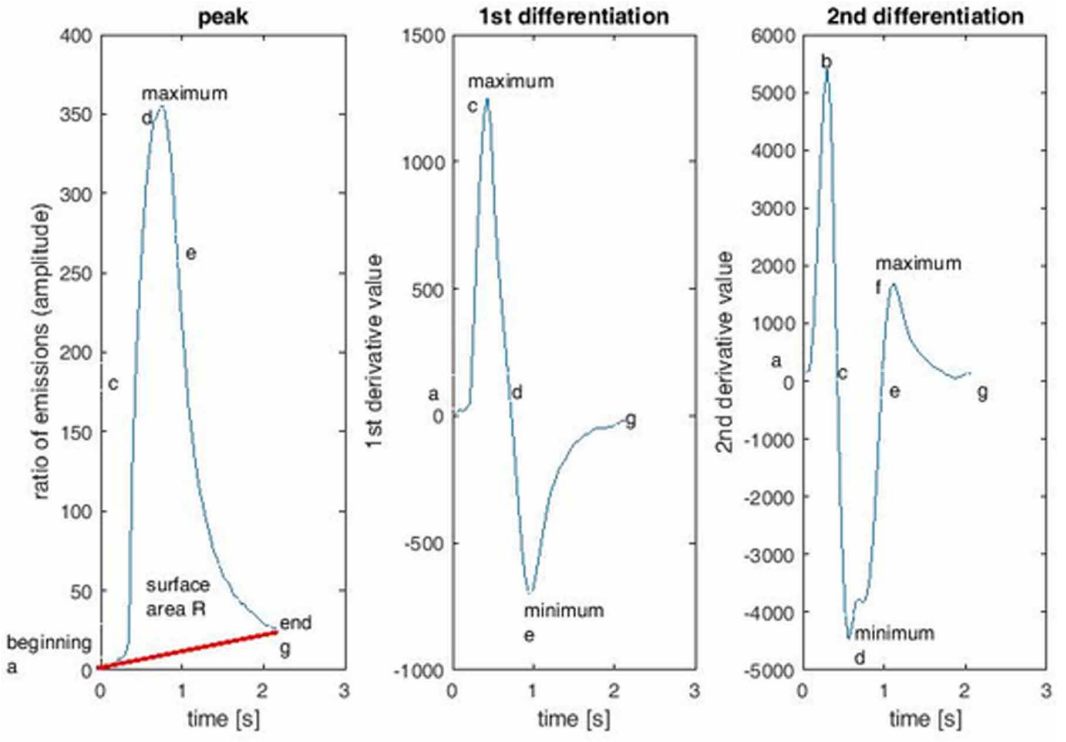

Table 2. Results of variable importance analysis with the Scatter analysis for 10 variables

Variable	Value
Amplitude of peak left side A_l	0.063
Amplitude of peak right side A_r	0.051
Duration of peak left side D_l [s]	0.133
Duration of peak right side D_r [s]	0.173
Maximum of the 1st derivative of peak left side $s´(c)$	0.066
Absolute minimum of the 1st derivative of peak right side $s´(e)$	0.055
Maximum of the 2nd derivative of peak right side $s´´(f)$	0.038
Absolute minimum of the 2nd derivative of right side $s´´(d)$	0.040
Surface area of peak R	0.082
Time difference from the current peak to the preceding one D_p [s]	0.189

in which n_j is the number of samples of the jth peak in the signal. The trapezoidal rule was employed in order to approximate the surface area of the definite integral determined by the nonlinear integrand signal $s(t)$, i.e., to calculate numerically the narrow interval spaces between the successive, discrete sample (amplitude) values. (The maximum or minimum of the 2nd derivative for the peak left side was not used since sometimes the duration of the left side was too short—but in a couple of samples only—for this purpose. Usually, the peak left side is narrower than the right side such as in Figure 5(a).)

Data Analysis Based on Peak Variables Applied

At first, we ran our Scatter analysis (Juhola & Siermala, 2012) to explore the importance of the 10 variables for the separation power between the two signal classes, i.e., normal and abnormal. The separation power value of all the data from [0,1) was 0.304, which predicts a high opportunity to separate the two signal classes. Scatter analysis results obtained for the 10 variables applied are shown in Table 2: the higher the value, the more important variable is for classification.

The results denote that the third, fourth, and tenth variables—i.e., the durations of the peak left and right sides and time difference between successive peaks—are more efficient in separating the two signal classes than the other variables. The other seven variables obtained low values, less than 0.1, predicting that they are less important but still useful. Peak surface area was slightly better than the other remaining variables. In general, no variable was highly predominant or very important with a scatter value, say, greater than 0.2. We have rarely obtained equally high values for other data sets (Juhola & Siermala, 2012). It is interesting that the three most important variables are directly time-dependent, and the best of all is the time difference of peak maximum (top) from that of the preceding peak or from the beginning of the signal in the case of the first peak in the signal.

Classification Tests and Results

The signal classification results obtained are presented in Tables 3-6. Each table has three parts: results for the whole data set of 438 signals, those separately for the high sampling frequency signals, and those for the low sampling frequency signals.

The tests were carried out on the basis of leave-one-out in which every single signal formed the test set, one by one, and the other signals formed the training set.

The classifiers implemented included *k*-nearest neighbor searching for odd *k* from 1 to 13, and linear, quadratic, and Mahalanobis discriminant analysis. In addition, support vector machines were run with several kernels (Marsland, 2015; Theodoridis & Koutroumbas, 2003; Webb, 2002).

Support vector machines (SVMs) (Cortes & Vapnik, 1995; Vapnik, 2000; Abe, 2010) are supervised machine learning methods that have shown great performance in many applications and have thus stabilized their position among researchers and practitioners. SVMs can be used to solve both classification and regression problems, but in this paper the focus is on classification. From the classification perspective, SVMs were originally designed for two-class classification tasks. However, various multi-class extensions have been developed later on, but these extensions are beyond the scope of this paper since we have only a binary classification problem between normal and abnormal transient signals. Original formulation of the SVM is based on quadratic programming optimization. We have applied a reformulation of the original SVM called Least-Squares Support Vector Machines (LS-SVM) in our study. LS-SVM was developed by Suykens et al. (1999a; 2002; 1999b) and the difference compared to the traditional SVM approach is in the hyperplane optimization and in the cost function, which is a 2-norm function whereas in Vapnik's SVM, the cost function is a form of 1-norm. Details related to hyperplane optimization can be found from the given references. The performance of the SVM is dependent on two issues: selection of the kernel function and parameter values. For this study, we selected seven kernels altogether: the linear and polynomial kernels with degrees from 2 to 6, and the radial basis function kernel.

Each of the kernels has parameters to be tuned up. For polynomial kernels (including the linear kernel), there is only a cost parameter, called the box constraint, C, to be optimized. The radial basis function (RBF) kernel instead has a box constraint and hyperparameter σ to be estimated. For both parameters, we selected the parameter value space to be $P=\{2^{-14}, 2^{-13}, \ldots, 2^{13}, 2^{14}, 2^{15}\}$. By these means, we tested polynomial kernels with 30 values and for RBF we performed a grid search where we tested all the pairs from the Cartesian product $P \times P$ (900 parameter value combinations). We performed leave-one-out cross-validation for all datasets (altogether six datasets) and repeated leave-one-out cross-validation with tested parameter values. As a selection criterion for the optimal parameter values, we used accuracy (the sum of the diagonal elements of a confusion matrix divided by the sum of all elements in a confusion matrix).

We used two approaches for determining the correct class labels for the signals. First, a biotechnology expert determined them independently of the peak recognition algorithm programmed and classification methods implemented. Second, the class labels of the signals were computed with the recognition and classification procedures programmed following the principle that a signal was classified as normal provided that all its peaks were computed to be normal—in other words, if one or more of its peaks were computed as abnormal, the entire signal was computed as abnormal.

In the training phase, the training of the classifier was made similarly for both the expert-vs.-algorithm and algorithm-vs.-algorithm approach. We trained our classifier using peak-based class labels (class labels for the peaks are obtained by the algorithm) and the training data corresponding to the peaks. There may be normal and abnormal peaks within an individual signal. When the leave-one-out procedure was done, we predicted class labels for each peak in the dataset.

After the training phase, we needed to obtain a confusion matrix and, hence, to evaluate the accuracy and other performance results. The training phase was conducted using peak-based information, but our classification task is a signal-level problem. Thus, obtaining the final classification result was a multi-stage process (in both the expert-vs.-algorithm and algorithm-vs.-algorithm approaches).

Expert-vs-Algorithm Approach

1. Determine a predicted class label for each signal. The determination of the predicted class label of the signal is made according to the following rule: If none of the predicted peak class labels

within an individual signal is abnormal, the predicted signal class label is normal. Otherwise, the class label is abnormal.

2. Make a comparison for each signal between the expert-based signal class and predicted signal class label. Determine a confusion matrix and evaluate accuracy and other performance measures.

Algorithm-vs-Algorithm Approach

1. Determine a predicted class label for each signal. The determination of the predicted class label of an individual signal is made according to the following rule: If none of the predicted peak class labels within an individual signal is abnormal, the predicted class label for the signal is normal. Otherwise, the class label for the signal is abnormal.

Table 3. Results after training with class labels (normal or abnormal) determined by the expert for all signals or their two subsets with classifiers of nearest neighbor searching of k in {1,3,5,7,9,11,13}, linear (LDA), quadratic (QDA), and Mahalanobis (Ma) discriminant analysis, where Se is sensitivity, Sp specificity, and Acc accuracy. The best accuracies are marked in bold.

Classifier	All 438 signals			High frequency 305 signals			Low frequency 133 signals		
	Se [%]	*Sp* [%]	*Acc* [%]	*Se* [%]	*Sp* [%]	*Acc* [%]	*Se* [%]	*Sp* [%]	*Acc* [%]
k=1	83	78	**80**	87	77	**82**	86	82	**84**
k=3	89	71	79	89	73	**82**	91	73	79
k=5	91	69	79	91	71	81	98	69	78
k=7	91	66	78	91	68	80	96	58	71
k=9	91	62	75	91	66	79	98	53	68
k=11	91	63	76	91	64	78	98	51	68
k=13	92	61	75	92	64	76	98	48	65
LDA	60	86	74	55	88	71	48	88	74
QDA	72	82	77	78	77	77	73	90	**84**
Ma	41	98	72	48	97	71	18	100	73

Table 4. Results after training with class labels (normal or abnormal) determined by the expert for all signals or their two subsets with support vector machine classifiers with linear, polynomial of degrees d, and radial basis function (RBF) kernels, where Se is sensitivity, Sp specificity, and Acc accuracy. The best accuracies are in bold.

Classifier	All 438 signals			High frequency 305 signals			Low frequency 133 signals		
	Se [%]	*Sp* [%]	*Acc* [%]	*Se* [%]	*Sp* [%]	*Acc* [%]	*Se* [%]	*Sp* [%]	*Acc* [%]
Linear	66	79	73	67	84	75	50	85	74
d=2	80	81	80	82	80	81	82	85	84
d=3	80	79	80	82	76	79	82	84	84
d=4	79	80	80	80	76	78	71	88	82
d=5	72	79	76	69	77	73	68	88	81
d=6	59	83	72	54	82	67	80	87	84
RBF	84	82	**83**	85	81	**83**	89	85	**87**

Table 5. Results after training with class labels (normal or abnormal) determined by the peak recognition algorithm for all signals or their two subsets with classifiers of nearest neighbor searching of k in {1,3,5,7,9,11,13}, linear (LDA), quadratic (QDA), and Mahalanobis (Ma) discriminant analysis, where Se is sensitivity, Sp specificity, and Acc accuracy. The best accuracies are marked in bold.

Classifier	All 438 signals			High frequency 305 signals			Low frequency 133 signals		
	Se [%]	*Sp* [%]	*Acc* [%]	*Se* [%]	*Sp* [%]	*Acc* [%]	*Se* [%]	*Sp* [%]	*Acc* [%]
k=1	94	97	**95**	100	100	**100**	89	94	**92**
k=3	96	86	91	98	92	95	89	81	84
k=5	97	81	89	97	85	92	98	78	87
k=7	97	80	89	98	83	92	96	58	71
k=9	97	76	87	98	81	91	100	62	77
k=11	97	75	87	98	80	90	100	59	76
k=13	98	74	86	99	79	90	100	56	74
LDA	58	89	73	55	93	72	42	89	69
QDA	75	92	83	84	91	87	67	95	84
Ma	38	100	68	47	100	70	15	100	65

Table 6. Results after training with class labels (normal or abnormal) determined by the peak recognition algorithm for all signals or their two subsets with support vector machine classifiers with linear, polynomial of degrees d, and radial basis function (RBF) kernels, where Se is sensitivity, Sp specificity, and Acc accuracy. The best accuracies are marked in bold.

Classifier	All 438 signals			High frequency 305 signals			Low frequency 133 signals		
	Se [%]	*Sp* [%]	*Acc* [%]	*Se* [%]	*Sp* [%]	*Acc* [%]	*Se* [%]	*Sp* [%]	*Acc* [%]
Linear	61	89	74	65	92	77	56	81	71
d=2	85	90	87	87	91	89	82	95	90
d=3	86	93	89	90	90	90	82	94	89
d=4	85	93	89	84	92	88	82	92	88
d=5	79	92	85	76	92	83	75	89	83
d=6	65	94	79	60	92	74	69	89	81
RBF	87	94	**91**	90	92	**91**	87	95	**92**

2. Determine a true class label for each signal based on the true peak class labels gained by the algorithm. The determination of the true class label of an individual signal is made according to the following rule: If none of the true peak class labels within an individual signal is abnormal, the class label for the signal is normal. Otherwise, the class label for the signal is abnormal.
3. Make a comparison for each signal between the true algorithm signal class and predicted algorithm signal class label. Determine a confusion matrix and evaluate accuracy and other performance measures.

Tables 3 and 4 show the classification results computed when the correct class labels, normal or abnormal, were given by the expert. Tables 5 and 6 show the classification results when we assumed that the peak classification procedure had given the correct class labels, normal or abnormal. The former was the expert-vs.-algorithm and the latter the algorithm-vs.-itself.

In Tables 3-6, sensitivity or the true positive rate and specificity or the true negative rate were computed so that the class of the normal were seen as positive and those of the abnormal as negative.

According to the results in Tables 3-6, the division of the signals into the two subsets of the high and low sampling frequencies did not improve them, but the situation varied method by method. In Table 3, the best classification method was nearest neighbor searching with *k* equal to 1, but in Table 4 the support vector machine with the radial basis function kernel exceeded it by 1–3% in accuracy. In Tables 5 and 6, the best method was nearest neighbor searching with *k* equal to 1, and the support vector machine with the radial basis function kernel and nearest neighbor with *k* equal 3 were the next best. Subject to sensitivity and specificity, the former were better classified by nearest neighbor searching, and the latter by the discriminant analysis methods and most support vector machines. The results in Tables 5 and 6 were better than those in Tables 3 and 4. This is natural, because the approach of the algorithm-vs.-itself for the results in Tables 5 and 6 were, of course, more favorable for the classification algorithm.

Table 7. Normal signals: variable means and standard deviations of each of the diseases LQT1, HCM, and CPVT with 487, 598, and 710 peaks in 28, 37, and 106 signals, respectively.

Variable	LQT1	HCM	CPVT
Amplitude of peak left side A_l	194±74	219±89	266±184
Amplitude of peak right side A_r	196±74	221±90	269±184
Duration of peak left side D_l [s]	0.369±0.208	0.282±0.143	0.494±0.27
Duration of peak right side D_r [s]	0.771±0.377	0.515±0.217	0.877±0.494
Maximum of the 1st derivative of peak left side $s´(c)$	876±436	2,268±948	1,644±1,088
Absolute minimum of the 1st derivative of peak right side $s´(e)$	544±209	1,111±428	897±547
Maximum of the 2nd derivative of peak right side $s´´(f)$	1,572±955	6,701±2,962	3,578±2,470
Absolute minimum of the 2nd derivative of right side $s´´(d)$	1,028±1,083	3,545±3,204	2,790±2971
Surface area of peak R	70.9±42.8	55.5±38.0	119.5±142.4
Time difference from the current peak to the preceding one D_p [s]	1.215±0.775	0.838±0.481	1.567±1.045

Table 8. Abnormal signals: variable means and standard deviations of each of the diseases LQT1, HCM, and CPVT with 1,143, 748, and 1,579 peaks in 62, 34, and 127 signals, respectively.

Variable	LQT1	HCM	CPVT
Amplitude of peak left side A_l	160±79	168±83	212±170
Amplitude of peak right side A_r	161±80	170±87	214±170
Duration of peak left side D_l [s]	0.335±0.216	0.216±0.145	0.309±0.202
Duration of peak right side D_r [s]	0.654±0.408	0.382±0.268	0.548±0.412
Maximum of the 1st derivative of peak left side $s´(c)$	789±485	1,766±835	1,212±1,033
Absolute minimum of the 1st derivative of peak right side $s´(e)$	493±277	1,003±496	772±535
Maximum of the 2nd derivative of peak right side $s´´(f)$	1,628±1,450	6,178±3,673	2,577±2,504
Absolute minimum of the 2nd derivative of right side $s´´(d)$	1,261±1,550	2,991±2,598	1,774±2,510
Surface area of peak R	52.3±39.8	32.4±29.5	68.8±72.3
Time difference from the current peak to the preceding one D_p [s]	1.147±0.979	0.621±0.427	0.936±0.794

Comparison Between Transient Signals of Disease-Specific iPSC-derived Cardiomyocytes

Our data set included cardiomyocytes associated with three diseases: LQT1, HCM, and CPVT. There were 90 signals from LQT1, 71 signals from HCM, and 233 signals from CPVT cardiomyocytes—394 in all. We left out 44 signals of controls from the original 438 signals, because their number was so small with only 13 abnormal signals. We were interested in exploring how the average variable values obtained differed among the signals of the cells for these three diseases. The means are shown in Table 7 for normal signals and in Table 8 for abnormal signals when the class labels were determined by the expert.

In both Tables 7 and 8, the differences between the three diseases are considerable. For every variable, we computed unpaired *t* tests between the three diseases, which gave 60 pairs for the three diseases, 10 variables, and two tables. All variables differed fairly statistically significantly between all disease pairs ($\alpha \leq 0.05$), and all but three pairs from Table 8 differed very significantly ($\alpha \leq 0.001$).

CONCLUSION

The classification of the entire calcium transient signals was performed with two different approaches: first the correct reference class labels of the transient signals were given by the biotechnology expert and, second, their correct class labels were determined based on the results produced by the peak recognition and classification. On one hand, we might assume that a human assessor is better at solving complicated classification tasks on the basis of extensive experience. On the other hand, we might also see the systematic approach of the computation as better, since the decisions of any human expert include slight variation over time. Overall, for the sake of these reasons, it is not guaranteed that the former approach is always the better approach. In any case, special software—in other words, efficient algorithms for the present classification task—will be needed to develop techniques for the analysis of massive numbers of iPSC-derived cardiomyocytes in medical laboratories in the future.

In the present research, we extended 56% our data set of calcium transient signals, added three new peak variables to our computation, ran our tests in more versatile ways, and obtained around 5% better classification accuracies compared to our previous tests (Juhola et al., 2015). In general, our results are promising and enable good opportunities to continue developing these classification methods and also to extend them to experiments with iPSC-derived cardiomyocytes exposed to different drugs. The results in Tables 7 and 8 in particular denote that it is possible to effectively separate the three diseases used in the experiment from each other. This shows that CPVT, LQT1, and HCM disease-

specific cardiomyocytes manifest the calcium cycling characteristics and pathophysiology of the specific disease. This could also indicate that it is possible to diagnose these diseases by analyzing only the calcium cycling of diseased cardiomyocytes. This observation is very promising and we just observed it to be true in our recent article (Juhola et al., 2018).

In the future, fast and automatic classification will accelerate the detection of cardiomyocyte calcium cycling abnormalities user-independently. Abnormally developed cardiomyocytes can be found and possibly dropped out from the cultured cells. This classification method will be required to analyze in-depth cardiomyocyte functionality that has been altered by different disorders, and will provide more information regarding the calcium cycling phenotype in these cells.

ACKNOWLEDGMENT

The second author wishes to thank the Finnish Cultural Foundation's Pirkanmaa Regional Fund, and the fourth author is grateful to the Academy of Finland and Finnish Cardiovascular Foundation for the financial support received.

REFERENCES

Abe, S. (2010). *Support Vector Machines for Pattern Classification* (2nd ed.). London, UK: Springer-Verlag. doi:10.1007/978-1-84996-098-4

Cortes, C., & Vapnik, V. (1995). Support-vector networks. *Machine Learning*, *20*(3), 273–297. doi:10.1007/BF00994018

Fatima, A., Xu, G., Shao, K., Papadopoulos, S., Lehmann, M., Arnáiz-Cot, J. J., & Šaric, T. et al. (2011). In vitro modeling of ryanodine receptor 2 dysfunction using human induced pluripotent stem cells. *Cellular Physiology and Biochemistry*, *28*(4), 579–592. doi:10.1159/000335753 PMID:22178870

Juhola, M., Joutsijoki, H., Penttinen, K., & Aalto-Setälä, K. (2018). Detection of genetic cardiac diseases by Ca^{2+} transient profiles using machine learning methods. *Scientific Reports*, *8*(1), 9355. doi:10.1038/s41598-018-27695-5 PMID:29921843

Juhola, M., Joutsijoki, H., Varpa, K., Saarikoski, J., Rasku, J., Iltanen, K., & Aalto-Setälä, K. et al. (2014). On computing calcium cycling anomalies in cardiomyocytes data. In *IEEE EMBS Conference,* Chicago, IL (pp. 1444-1447). IEEE.

Juhola, M., Penttinen, K., Joutsijoki, H., Varpa, K., Saarikoski, J., Rasku, J., & Aalto-Setälä, K. et al. (2015). Signal analysis and classification methods for the calcium transient data of stem cell-derived cardiomyocytes. *Computers in Biology and Medicine*, *61*, 1–7. doi:10.1016/j.compbiomed.2015.03.016 PMID:25841082

Juhola, M., & Siermala, M. (2012). A scatter method for data and variable importance evaluation. *Integrated Computer-Aided Engineering*, *19*(2), 137–149. doi:10.3233/ICA-2011-0385

Jung, C. B., Moretti, A., Mederos y Schnitzler, M., Iop, L., Storch, U., Bellin, M., & Laugwitz, K.-L. et al. (2012). Dantrolene rescues arrhythmogenic RYR2 defect in a patient-specific stem cell model of catecholaminergic polymorphic ventricular tachycardia. *EMBO Molecular Medicine*, *4*(3), 180–191. doi:10.1002/emmm.201100194 PMID:22174035

Kiviaho, A. L., Ahola, A., Larsson, K., Penttinen, K., Swan, H., Pekkanen-Mattila, M., & Aalto-Setälä, K. et al. (2015). Distinct electrophysiological and mechanical beating phenotypes of long QT syndrome type 1-specific cardiomyocytes carrying different mutations. *IJC Heart & Vasculature*, *8*, 19–31. doi:10.1016/j.ijcha.2015.04.008 PMID:28785673

Kujala, K., Paavola, J., Lehti, A., Larsson, K., Pekkarinen-Mattila, M., Viitasalo, M., & Aalto-Setälä, K. et al. (2012). Cell model of catecholaminercig polymorphic ventricular tachycardia reveals early and delayed after depolarizations. *PLoS One*, *7*(9), e44660. doi:10.1371/journal.pone.0044660 PMID:22962621

Lan, F., Lee, A. S., Liang, P., Sanchez-Freire, V., Nguyen, P. K., Wang, L., & Wu, J. C. et al. (2013). Abnormal calcium handling properties underlie familial hypertrophic cardiomyopathy pathology in patient-specific induced pluripotent stem cells. *Cell Stem Cell*, *3*(1), 101–113. doi:10.1016/j.stem.2012.10.010 PMID:23290139

Marks, A. R. (2013). Calcium cycling proteins and heart failure: Mechanisms and therapeutics. *The Journal of Clinical Investigation*, *123*(1), 46–52. doi:10.1172/JCI62834 PMID:23281409

Marsland, S. (2015). *Machine Learning, An Algorithmic Perspective* (2nd ed.). Boca Raton, FL: CRC Press.

Ojala, M., Prajapati, C., Pölönen, R. P., Rajala, K., Pekkanen-Mattila, M., Rasku, J., & Aalto-Setälä, K. et al. (2016). Mutation-specific phenotypes in hiPSC-derived cardiomyocytes carrying either myosin-binding protein C or α-Tropomyosin Mutation for Hypertrophic Cardiomyopathy. *Stem Cells International*. PMID:27057166

Penttinen, K., Siirtola, H., Ávalos-Salguero, J., Vainio, T., Juhola, M., & Aalto-Setälä, K. (2015b). Novel analysis software for detecting and classifying Ca^{2+} transient abnormalities in stem cell-derived cardiomyocytes. *PLoS One*, *10*(8), e0135806. doi:10.1371/journal.pone.0135806 PMID:26308621

Penttinen, K., Swan, H., Vanninen, S., Paavola, J., Lahtinen, A. M., Kontula, K., & Aalto-Setälä, K. (2015a). Antiarrhythmic effects of Dantrolene in patients with catecholaminergic polymorphic ventricular tachycardia and replication of the responses using iPSC models. *PLoS One*, *10*(7), e0134746. doi:10.1371/journal.pone.0134746 PMID:26230682

Suykens, J. A. K., van Gestel, T., De Brabanter, J., De Moor, B., & Vandewalle, J. (2002). *Least Squares Support Vector Machines*. New Jersey, USA: World Scientific. doi:10.1142/5089

Suykens, J. A. K., & Vandewalle, J. (1999a). Least squares support vector machines. *Neural Processing Letters*, *9*(3), 293–300. doi:10.1023/A:1018628609742

Suykens, J. A. K., & Vandewalle, J. (1999b). Multiclass least squares support vector machines. *Proceedings of International Joint Conference on Neural Networks*, *2*, 900–903. doi:10.1109/IJCNN.1999.831072

Takahashi, K., Tanabe, K., Ohnuki, M., Narita, M., Ichisaka, T., Tomoda, K., & Yamanaka, S. (2007). Induction of pluripotent stem cells from adult human fibroblasts by defined factors. *Cell*, *131*(5), 861–872. doi:10.1016/j.cell.2007.11.019 PMID:18035408

Theodoridis, S., & Koutroumbas, K. (2003). Pattern Recognition (2nd ed.). San Diego, CA: Academic Press.

Vapnik, V. (2000). *The Nature of Statistical Learning Theory* (2nd ed.). New York, USA: Springer-Verlag. doi:10.1007/978-1-4757-3264-1

Webb, A. (2002). *Statistical Pattern Recognition* (2nd ed.). Chichester, UK: John Wiley & Sons. doi:10.1002/0470854774

Martti Juhola received his M.Sc. and Ph.D. degrees in 1982 and 1987 from computer science at the University of Turku, Finland, where he was an assistant, lecturer and researcher in 1980-92. During 1992-97 he was professor of computer science at the University of Kuopio and since 1997 at the Tampere University, Finland. His research interest includes data mining, signal analysis and pattern recognition particularly with medical applications.

Henry Joutsijoki received his M.Sc. and Phil.Lic. degrees in mathematics from the University of Tampere in 2008 and 2010. In 2012 he received Ph.D. degree in computer science and is a member of Data Analysis Research Group at the Faculty of Natural Sciences. In 2017, Henry Joutsijoki received the degree of Adjunct Professor. His research interests include machine learning, support vector machines and data mining.

Kirsi Varpa made her MSc Degree in computer sciences at University of Tampere in the year 2005 and her PhD in 2019 on the topic of knowledge discovery experimented with otoneurological data. She has participated research projects concerning decision support system, machine learning, data mining and knowledge discovery handling medical data. Currently, she works as Senior Adviser in the Development, Quality and Operations at the Tampere University of Applied Sciences.

Kirsi Penttinen is currently a post doc researcher in the Faculty of Medicine and Life Sciences at the University of Tampere. Her research interest lies in the area of stem cell derived cardiac disease models and their functional properties, specifically in cardiac calcium handling. She earned her Master of Science (Tech.) in Biomaterials from Tampere University of Technology in 2010 and Doctor of Science (Tech.) in Biomedical Engineering from Tampere University of Technology in 2016.

Katriina Aalto-Setälä, M.D. is the Professor of Physiology at the Faculty of Medicine and Life Sciences, University of Tampere and a cardiologist at the Heart Hospital, Tampere University Hospital, Tampere, Finland. She is an invasive cardiologist and in charge of the genetic cardiac out-patient clinic. Dr. Aalto-Setälä did her postdoctoral training at the Rockefeller University, New York in Prof. John Breslow's laboratory and also spent a year in Prof. Malcolm Brenner's laboratory at St Jude Children's Hospital, Memphis TN. Later, she spent a year as a visiting Professor at the Gladstone Institutes in Prof. Bruce Conklin's laboratory and learned the iPSC technology in Prof. Shinya Yamanaka's laboratory. Additionally, she has spent time in Prof Andrew Mark's group in New York and in Prof. Mark Mercola's group at Stanford. Her research focuses on genetic cardiac diseases such as genetic arrhythmias and atherosclerosis with the help of induced pluripotent stem cell (iPSC) technology. The main aim of the research group is to learn more about the basic pathology of the genetic diseases. Her research group in collaboration with researches at the Tampere Technical University has also invented new methods to monitor and analyze the maturity and functionality cardiomyocytes.